Biochimica et Biophysica Acta 1808 (2011) 1639–1644

Contents lists available at ScienceDirect

Biochimica et Biophysica Acta

journal homepage: www.elsevier.com/locate/bbamem

Structure and metal ion binding of the first transmembrane domain of DMT1

Dan Wang, Yuande Song, Jiantao Li, Chunyu Wang, Fei Li *

State Key Laboratory of Supramolecular Structure and Materials, Jilin University, 2699 Qianjin Avenue, Changchun 130012, People's Republic of China

ARTICLE INFO

Article history:
Received 25 September 2010
Received in revised form 3 November 2010
Accepted 4 November 2010
Available online 11 November 2010

Keywords:
DMT1-TMD1
Structure
Topology
Metal ion binding
NMR

ABSTRACT

DMT1 is an integral membrane protein with 12 putative transmembrane domains. As a divalent metal ion transporter, it plays an important role in metal ion homeostasis from bacteria to human. Loss-function mutations at the conserved motif DPGN located within the first transmembrane domain (TMD1) of DMT1 indicate the significance of TMD1 in the biological function of the protein. In the present work, we study the structure, topology and metal ion binding of DMT1-TMD1 peptide by nuclear magnetic resonance using sodium dodecyl sulfate and dodecylphosphocholine micelles as membrane mimics. We find that the peptide forms an α-helix-extended segment–α-helix configuration in which the motif DPGN locates at the central flexible region. The N-terminal part of the peptide is deeply embedded in micelles, while the motif section and the C-terminal part are close to the surface of micelles. The peptide can bind to Mn^{2+} and Co^{2+} ions by the side chains of the negatively charged residues in the motif section and the C-terminal part of TMD1. The crucial role of the central flexible region and the C-terminal part of TMD1 in metal ion capture is confirmed by the binding of the N-terminal part truncated TMD1 to metal ions.

1. Introduction

Iron is thought to be transported into cells by transferrin-receptor-mediated endocytosis in blood plasma [1,2]. Failure to maintain appropriate levels of iron in humans will lead to iron-deficiency anemia and certain neurodegenerative diseases [3,4]. Several genes related to iron homeostasis have been identified. DMT1 (divalent metal ion transporter 1), also known as DCT1 (divalent cation transporter 1), Nramp2 (natural resistance-associated macrophage protein 2) or Slc11a2 (solute carrier family 11 member 2) [5–7], is one of these genes. It is expressed at the brush border of the duodenum where it mediates uptake of dietary iron with pH coupled fashion, stimulated by acidic pH [8,9]. Besides Fe^{2+}, DMT1 can transport Mn^{2+}, Zn^{2+}, Cu^{2+}, Ni^{2+}, Co^{2+}, Pb^{2+} and Cd^{2+} ions [10].

DMT1 is an integral protein and contains 12 putative transmembrane domains (TMDs) with both N- and C-terminus located in the cytoplasm and two putative glycosylation sites in an extracytoplasmic loop [11]. Of the twelve TMDs, TMD1 (defined according to the delimitation of Czachorowski et al. [12] for sequence alignment of Slc11 homologues, the extracellular loop1 defined in 1995 [13] is included in this TMD1) was demonstrated to be one of the TMDs crucial for the metal ion transport of the protein [14–16]. The specific motif DPGN in TMD1 is conserved in all transporters of Slc11 family and appears to be essential for function. It was revealed that both the conservative substitutions of Asp86 and the mutations of Gly88 (G88A, C, V) in the signature sequence of DMT1 result in complete loss of transport activity [15,16]. The conservative substitutions were also carried out in the previous study of MntH, a homolog of DMT1 in *Escherichia coli*, for all four residues in the motif and it was found that all of these mutants are severely defective in $^{54}Mn^{2+}$ transport [14]. The nonconserved amino acid residues Asp93 and Gln95 in TMD1 were also found to be involved in the metal ion transport of DMT1, and the transport activity was decreased by the replacement of D93A and even abolished by Q95D [16]. On the basis of these biological results, we recently investigated the interactions of a 12-mer peptide from the N-terminal part truncated DMT1-TMD1 (previously defined as exo-loop1 according to the definition of Cellier et al. [13]) with metal ions and revealed that the isolated segment can specifically bind divalent metal ions mainly by coordination of side chains of the negatively charged residues (Asp86, Glu91 and Asp93) [17].

Recently, the three-dimensional structures of SLC11 proteins were modeled based on the LeuT/SLC6 crystal structure [12,18]. According to this model, TMD1 forms a discontinuous helix (α-helix-extended peptide–α-helix) structure. In the present work, we further studied the peptides corresponding to entire DMT1-TMD1 and its N-terminal part truncated segment in micelle associated state using NMR spectroscopic technique to explore the structures, topologies and metal ion binding of these peptide segments. We first confirmed experimentally an α-helix-extended segment–α-helix structure of DMT1-TMD1 in membrane-mimetic environments and found the key role of the negatively charged residues in the C-terminal part of TMD1 for metal ion binding.

* Corresponding author. Tel.: +86 431 85168548; fax: +86 431 85193421.
E-mail address: feili@jlu.edu.cn (F. Li).

0005-2736/$ – see front matter © 2010 Elsevier B.V. All rights reserved.
doi:10.1016/j.bbamem.2010.11.005

2. Materials and methods

2.1. Materials

The peptides used in this study (Table 1) were synthesized and purified by GL Biochem (Shanghai) Ltd. The purity is estimated by mass spectroscopy to be >95%. Deuterated sodium dodecyl sulfate (SDS-d_{25}; 98%), deuterated dodecylphosphocholine (DPC-d_{38}; 98%) and D_2O (99.8%) were purchased from Cambridge Isotope Laboratories. The spin label 16-doxyl-stearic acid (16-DSA) was obtained from Sigma. The peptides and chemical agents were used as purchased without further treatment.

2.2. Sample preparation

Certain amounts of peptide and detergent (SDS-d_{25} or DPC-d_{38}) were separately dissolved into 225 μL deionized water. After they were mixed, the volume of 50 μL D_2O was added in the mixture to obtain a sample of 2 mM peptide and 240 mM detergent in 0.5 mL H_2O/D_2O (90%/10% v/v). The pH values of samples were adjusted by adding a small amount of NaOH or HCl solution. Stock solutions of $MnCl_2$ (12 mM) and $CoCl_2$ (50 mM) were prepared by dissolving certain amounts of salts in deionized water.

2.3. NMR spectroscopy

NMR spectra were performed on a Bruker Avance 500 spectrometer at 298 K. The samples were added in 5 mm tubes using 3-(trimethylsilyl)-propionate-2, 2, 3, 3-d_4 (TSP) as an internal standard. The NOESY spectra were recorded with a mixing time of 200 ms and the TOCSY spectra were acquired using the MLEV-17 pulse sequence [19] with mixing time of 100 ms. The WATERGATE technique was applied in both the TOCSY and NOESY experiments for water signal suppression [20,21]. Typically, 2 K data points in F2 and 512 increments in F1 dimension were collected with scans of 48 for each increment and a relaxation delay of 2 s. The 2D NMR spectra were processed using standard Bruker software (XWINNMR Version 3.5) and analyzed using software SPARKY [22]. The effects of 16-doxyl-stearic acids and paramagnetic Mn^{2+} and Co^{2+} ions on the NMR signals were monitored by recording NOESY spectra in the absence and presence of the spin label (the molar ratio of SDS:16-DSA was 60:1 which approximately corresponds one spin-label per micelle) and the metal ions (the molar ratios of peptide/ion were 67:1 for the addition of Mn^{2+} in peptide/SDS-d_{25} sample, 3.3:1 and 1.8:1 for the addition of Co^{2+} in peptide/SDS-d_{25} and peptide/DPC-d_{38} samples, respectively).

2.4. Structure calculation

The structural calculations of the micelle-bound peptides were carried out using the program CYANA (1.0.6) [23]. The NOE intensities and chemical shifts were served as input data. The NOE intensities were transformed into distance restraints with the CALIBA program. These distance restraints were subjected to local conformational analyses using the GRIDSEARCH. Structure calculations were initiated from 200 randomized conformers and the 20 structures with the lowest target functions were further refined by energy minimization with the AMBER7 program [24] under the force field of Cornell et al. [25] using a generalized Born solvent model. Structural analysis and visualization were achieved by the PROCHECK-NMR program [26] and MOLMOL program [27], respectively.

Table 1
Sequences of the peptides studied.

Name	Sequence[a]
TMD1	R^{1}KLWAFTGPG FLMSIAYLD^{19}P GNIESDLQSG^{30}
TMD1–D19A	R^{1}KLWAFTGPG FLMSIAYLA^{19}P GNIESDLQSG^{30}
TMD1–D26A	R^{1}KLWAFTGPG FLMSIAYLD^{19}P GNIESALQSG^{30}
Nt-TMD1-loop1/2	D^{19}P GNIESDLQSG^{30} AVAGFKLLW^{39}

[a] The amino acid sequences of TMD1 and Nt-TMD1-loop1/2 (Nt: N-terminal truncated; loop1/2: the region between the C-terminal end of TMD1 and the N-terminal end of TMD2) correspond to the segments 68–97 and 86–106 of DMT1, respectively [12].

3. Results

3.1. Structure

We first recorded the NOESY spectra of TMD1 incorporated with SDS-d_{25} and DPC-d_{38} micelles at both 298 and 283 K (pH 4). We found that the chemical shifts of the spectra are slightly changed at the two temperatures, but the signals are broadened at lower temperature. Therefore, we measured the 2D TOCSY and NOESY spectra of the samples at 298 K. Furthermore, we found that the Hα chemical shifts of the peptide in SDS-d_{25} micelles are little influenced by pH values. This suggests that the secondary structure of the peptide is little influenced by solution pH. Therefore, we used the spectroscopic data of the peptide TMD1 in SDS-d_{25} micelles at pH 5.5 and the peptide in DPC-d_{38} micelles at pH 3.5 for determination of the structures of the peptide in these media. In these pH conditions, the 2D spectra of the peptide displayed the best dispersion.

The TOCSY and NOESY spectra of 2 mM peptide in 240 mM SDS-d_{25} micelles at pH 5.5 were recorded at 298 K and assigned, and the NOE connectivities were obtained from the NOESY spectrum (see Fig. S1 in Supplementary materials). The structure calculation based on these NOE restraints defines two α-helical spans over Leu12–Ile15 and Ile23–Asp26 kinked by a flexible portion, namely an 'α-helix-extended segment–α-helix' conformation (Fig. 1). The NMR restraints used in calculations and structural statistics extracted from calculation results are listed in Table 2. The backbone dihedral angles of all α-helices are well-defined as assessed by PROCHECK-NMR. Over 80% of the residues occupy the most favorable region of the Ramachandran plot and no residues are found in the disallowed region. Similar results were obtained for the peptide in DPC-d_{38} micelles (see Figs. S2 and S3 in Supplementary materials), and an 'α-helix-extended segment–α-helix' structure with two α-helical stretches from Leu12 to Tyr17 and Ile23 to Leu27 is well defined.

Two Asp residues, one in the central flexible region of the TMD1 peptide and the other within the helix of the C-terminal part, were assumed to be crucial for the binding of Slc11 proteins to metal ions and the coupling with protons in the transport process [16]. Therefore, we examined the structures of two mutants of TMD1, D19A and D26A, in SDS-d_{25} micelles at pH 5.5, 298 K. Both NOE connectivities (see Figs. S4 and S5 in Supplementary materials) and calculated structures based on the NOE restraints (Fig. 2) demonstrate that the mutations of these two Asp residues have no obvious effect on the structure of the peptide.

The structure of the N-terminal part truncated peptide Nt-TMD1-loop1/2 which is closely related to the ion binding of DMT1 was also studied in SDS-d_{25} micelles at pH 5.5 by NMR (see Fig. S6 in Supplementary materials). This peptide in SDS-d_{25} micelles forms an α-helix from Glu24 to Leu37 with a flexible N-terminus (Fig. 3). The sequence between the C-terminal end of TMD1 and the N-terminal end of TMD2 (loop1/2) provides additional hydrophobic interaction with micelle, inducing a continuous α-helix structure in the segment Nt-TMD1-loop1/2.

3.2. Topology

The spin labeled 16-DSA, when incorporated into micelles, selectively broadens the resonances of residues close to the center of micelle, corresponding to the apolar end of the carbon chain [28],

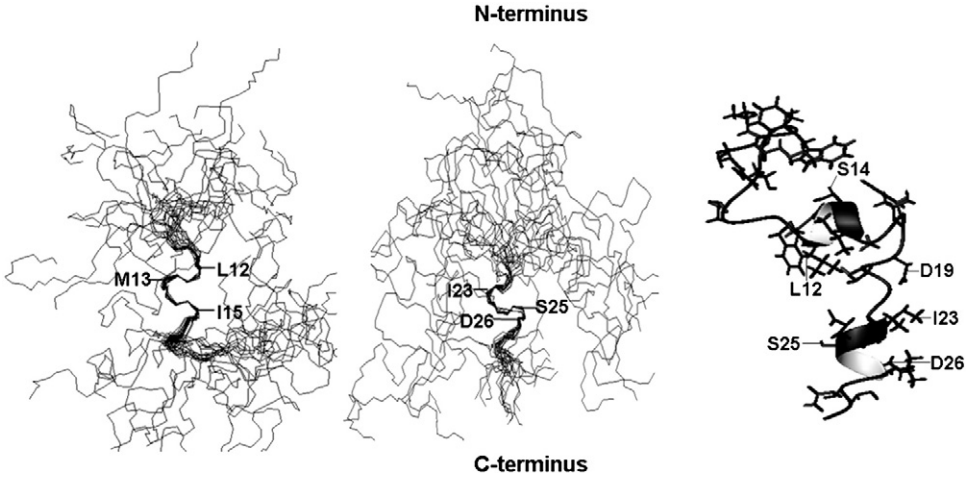

Fig. 1. Ensemble of backbone atoms of 20 structures with the lowest target functions fitted over Leu12–Ile15 (left) and Ile23–Asp26 (middle) and a ribbon representation (right) for TMD1 in SDS-d_{25} micelles at pH 5.5.

while paramagnetic metal ion Mn^{2+} in solution broadens the NMR signals of the solvent-exposed residues [29]. In this study, the intensities of the cross-peaks in the NOESY spectra were used to estimate the effects of the paramagnetic agents on micelle-associated TMD1 peptide. In the presence of 16-DSA, the cross-peak intensities of Leu3, Trp4 and Ala5 near the N-terminus of the peptide and Tyr17 and Leu18 in the central region of the peptide are largely quenched, while the cross-peak intensities of the residues from Pro20 to the C-terminal end and the residues Thr7–Ala16 are less or moderately broadened (Fig. 4). On the other hand, the addition of Mn^{2+} leads to evident broadening of the cross-peaks from the residues of the C-terminal part (Ala16–Ser29), while the cross-peaks from the residues of the N-terminal part are less affected by Mn^{2+} (Fig. 5). The combination of both 16-DSA and Mn^{2+} results suggests that the N-terminal part (including helix I) of the peptide TMD1 is embedded in SDS micelles, while the C-terminal part (including helix II) is close to the surface of the micelles.

Table 2
Statistics of 20 structures with the lowest target functions for the peptide TMD1 in SDS micelles at pH 5.5, 298 K.

Average target functions ($Å^2$)	0.36 ± 0.09
Number of nonredundant distance restraints	255
Intraresidual ($\|i-j\|=0$)	108
Sequential ($\|i-j\|=1$)	108
Medium ($\|i-j\| \le 4$)	39
Long range ($\|i-j\|>4$)	0
Average sum of distance restraint violations (Å)	2.40 ± 0.40
Average maximum distance restraint violation (Å)	0.29 ± 0.08
Average sum of torsion angle restraint violations (°)	0.20 ± 0.40
Average maximum of torsion angle restraint violation (°)	0.21 ± 0.38
AMBER energy (kcal mol^{-1})	-1012.61 ± 0.65
Rms deviation from the mean structure (Å)	
Well-defined residues (Å)	
Backbone heavy atoms	0.17 ± 0.10 (N)[a]
	0.37 ± 0.26 (C)[a]
All heavy atoms	1.18 ± 0.40 (N)[a]
	1.38 ± 0.47 (C)[a]
Ramachandran plot statistics (for each helical span)	
Residues in most favored region (%)	83.8
Residues in additionally allowed region (%)	15.6
Residues in generously allowed region (%)	0.6
Residues in disallowed region (%)	0

[a] N and C in the parentheses represent the helical span in the N-terminal and C-terminal part of the peptide, respectively.

3.3. Metal ion binding

In Mn^{2+} experiment of TMD1, one can also find that the cross-peaks associated with the side chain protons of Asp19 and Asp26 and the cross-peaks associated with the backbone protons of Asn22 are much more broadened than those of other residues in the C-terminal part (Fig. 5). Because Mn^{2+} is one of the divalent metal ions that DMT1 can transport, the specific resonance broadening of the three residues may imply that these residues are involved in the binding to Mn^{2+}. Because the paramagnetic effect of Mn^{2+} is strong, only small amount of Mn^{2+} ions ([peptide]/[Mn^{2+}] = 67:1) were added in solution. As a result, the change in the chemical shift induced by the metal ion was not observed in the NMR spectra of the peptide sample.

The interaction of the peptide with Co^{2+} was further probed. Co^{2+} is also a paramagnetic ion, but its paramagnetic effect is much smaller than Mn^{2+}. Therefore, larger amount of Co^{2+} was added into micelle solution of the peptide ([peptide]/[Co^{2+}] = 3.3:1 for SDS-d_{25} sample and 1.8:1 for DPC-d_{38} sample). The addition of Co^{2+} in micelle solution of TMD1 not only dramatically broadens the cross-peaks associated with the β-protons of the residues Asp19 and Asp26 (Fig. 6), but also induces evident down-field shifts of the β-protons of the two Asp residues and the γ-protons of Glu24 (Fig. 7), while both the intensity and chemical shift of the NMR signals from other residues are less affected. These results indicate that the residues Asp19, Glu24 and Asp26 (corresponding to Asp86, Glu91 and Asp93 in

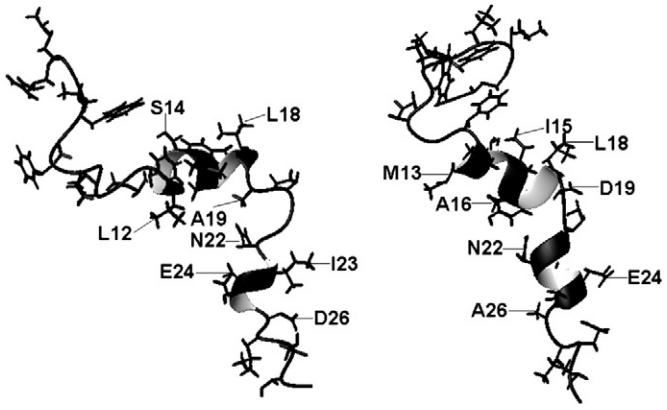

Fig. 2. Ribbon representations of D19A (left) and D26A (right) in SDS-d_{25} micelles at pH 5.5.

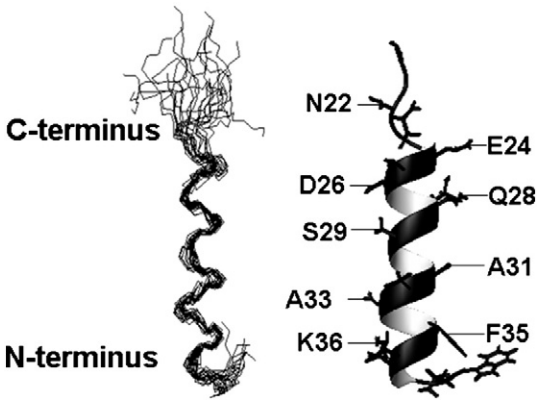

Fig. 3. Ensemble of backbone atoms of 20 structures with the lowest target functions fitted over Glu24–Leu37 (left) and ribbon representation of their mean structure (right) for Nt-TMD1-loop1/2 in SDS-d_{25} micelles at pH 5.5.

DMT1) may be involved in the coordination with the metal ion by the carboxyl groups of their side chains. In order to verify the crucial role of the side chains of two Asp residues in the binding to Co^{2+}, we made substitution of Ala for each Asp residue and compared the intensities of the NOESY spectra in the absence and presence of Co^{2+} (Fig. 8). The remarkable broadening of either Asp26 or Asp19 resonance remains in the NOESY spectrum of D19A or D26A, but the peak broadening of the substituted one is completely abolished. In addition, an evident downfield shifting of the γ-protons of Glu24 was also observed in the NOESY spectrum of each mutant. It is further suggested that the side chains but not the backbone atoms of the two Asp residues provide the coordination sites to Co^{2+}. When one Asp residue is substituted, the other one can also interact with the metal ion possibly by the aid of H_2O molecules which replace the carboxyl oxygen atoms of the substituted Asp to coordinate with metal ions.

The interaction of Co^{2+} with the N-terminal part truncated peptide Nt-TMD1-loop1/2 in SDS-d_{25} micelles was also analyzed by observing the effect of Co^{2+} on the intensity and chemical shift of NMR signals of the peptide. In the NOESY spectrum, the specific broadening of the cross peaks associated with side chain protons of Asp19, Glu24 and Asp26 is induced by Co^{2+} along with a downfield shift of the β-protons of Asp19 and Asp26 and the γ-protons of Glu24 (Figs. 9 and 10), suggesting that the peptide Nt-TMD1-loop1/2 binds to Co^{2+} by the side chains Asp19, Glu24 and Asp26, a coordination fashion similarly to that of entire TMD1 peptide.

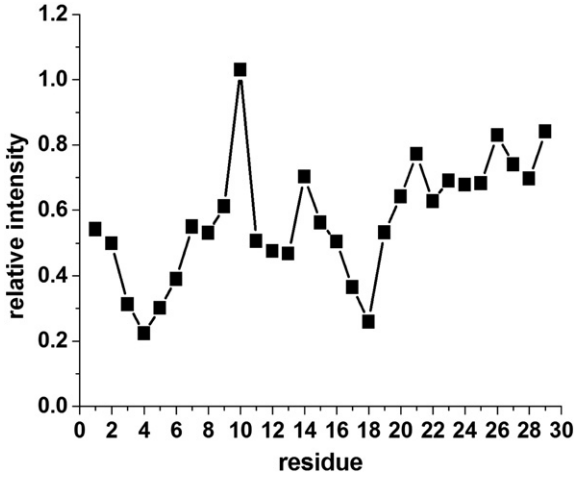

Fig. 4. Intensity of the most quenched cross-peak of each residue in the NOESY spectrum of TMD1 in SDS-d_{25} micelles incorporated with 16-DSA relative to that without the spin label at pH 5.5.

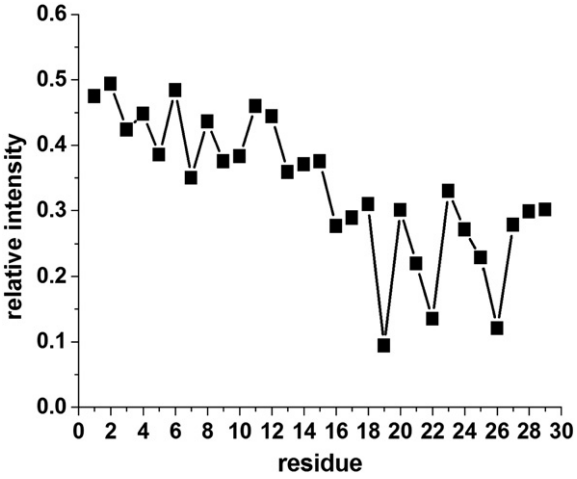

Fig. 5. Intensity of the most quenched cross-peak of each residue in the NOESY spectrum of TMD1 in SDS-d_{25} micelles at pH 5.5 in the presence of Mn^{2+} relative to that in the absence of the metal ion.

4. Discussion

In the previous study, an architecture model of Slc11 transporter deduced from homology threading and structure refining based on the crystal structures of LeuT/SLC6 suggests an important role of the most conserved elements of the Slc11 hydrophobic core, TMD1, 3, 6 and 8, in the metal ion uptake of DMT1. According to the model, the protein forms an anti-parallel symmetrical structure in which TMD1 and TMD6 are similarly folded but in inverted orientation with respect to the membrane and the conserved motifs Asp–Pro–Gly and Met–Pro–His located respectively between TMD1a/b and TMD6a/b form anti-parallel "TM helix/extended peptide" boundaries, lining a "pore" cavity and enabling H^+-dependent divalent metal ion transport [12,18]. Our previous study of DMT1-TMD6 in SDS micelles has established that TMD6 folds as an 'α-helix-extended segment–α-helix' structure with the motif HPM falling in the flexible central part of the transmembrane peptide [30]. In the present study, we first experimentally verify that TMD1 also forms the 'α-helix-extended segment–α-helix' structure, similarly to TMD6. The motif Asp–Pro–Gly–Asn (DPGN) locates between two helix segments which belong to TMD1a (in the N-terminal region of TMD1) and TMD1b (in the C-terminal region of TMD1) [12,18]. The part of TMD1a is embedded in a deeper position of micelles, while the DPGN motif and TMD1b locate close to the surface of micelles. Because of its flexibility, the motif

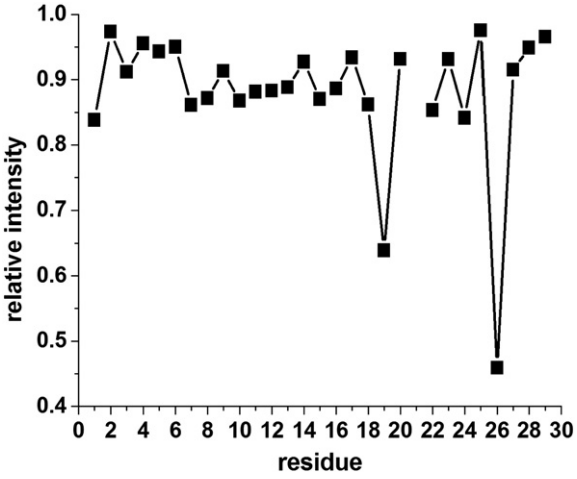

Fig. 6. Intensity of the most quenched cross-peak of each residue in the NOESY spectrum of TMD1 in SDS-d_{25} micelles at pH 5.5 in the presence of Co^{2+} relative to that in the absence of the metal ion.

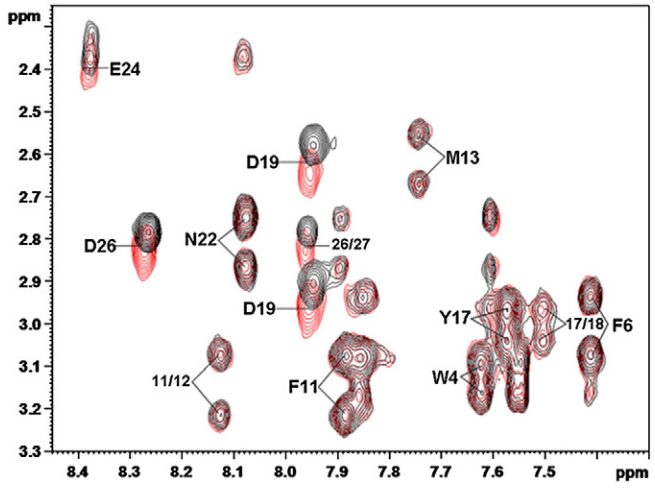

Fig. 7. Hβ-HN region of the NOESY spectrum of TMD1 in SDS-d_{25} micelles at pH 5.5 in the absence (black) and the presence (red) of Co^{2+}.

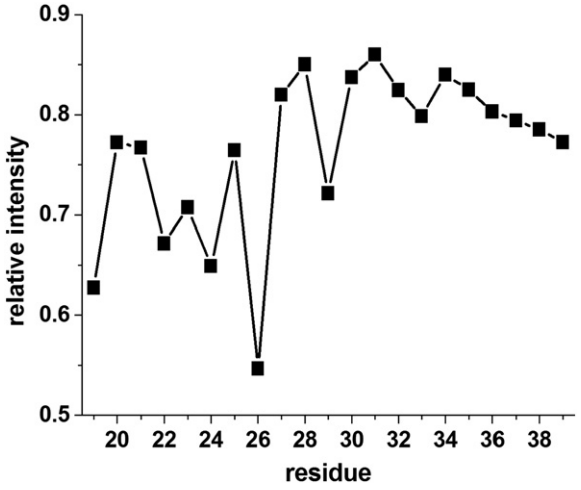

Fig. 9. Intensity of the most quenched cross-peak of each residue in the NOESY spectrum of Nt-TMD1-loop1/2 in SDS-d_{25} micelles at pH 5.5 in the presence of Co^{2+} relative to that in the absence of the metal ion.

DPGN may undergo fast and subtle conformational change in response to pH through the regulation of the relative orientation and position between two helix stretches and thus be important for opening size of the pore and the accommodation of divalent metal ions in a tightly packed α-helical bundle. The residue Asp19 (corresponding to Asp86 in DMT1) in the motif and the negatively charged residues in TMD1b, such as Glu24 (Glu91 in DMT1) and Asp26 (Asp93 in DMT1), were found to be involved in the coordination of DMT1 to Mn^{2+} and Co^{2+} in this study. The parallel mutational studies of positions Asp86, Gly88, Asp93 and Gln95 from the Slc11a2 have led to the suggestion that this region may form part of metal ion binding site in the protein [15,16,18,31].

The importance of the motif DPGN and TMD1b in metal ion binding of TMD1 was further confirmed by the interactions of divalent metal ions with two N-terminal part truncated peptides, a 12-mer peptide DPGNIESDLQSG (Nt-TMD1) and a 21-mer peptide Nt-TMD1-loop1/2, both peptides include TMD1b segment. Although the truncation of TMD1a from TMD1 leads to unfolding of helix of TMD1b, we still found the binding of the truncated peptide Nt-TMD1 to divalent metal ions (including Mn^{2+}, Co^{2+}, Cu^{2+}, Ni^{2+} and Fe^{2+}) in aqueous solution by the coordination of the negatively charged residues Asp19, Glu24 and Asp26 [17]. The extension of the Nt-TMD1 to the N-terminal end of TMD2 (Nt-TMD1-loop1/2) recovers the structure of the extended segment-helix and results in the

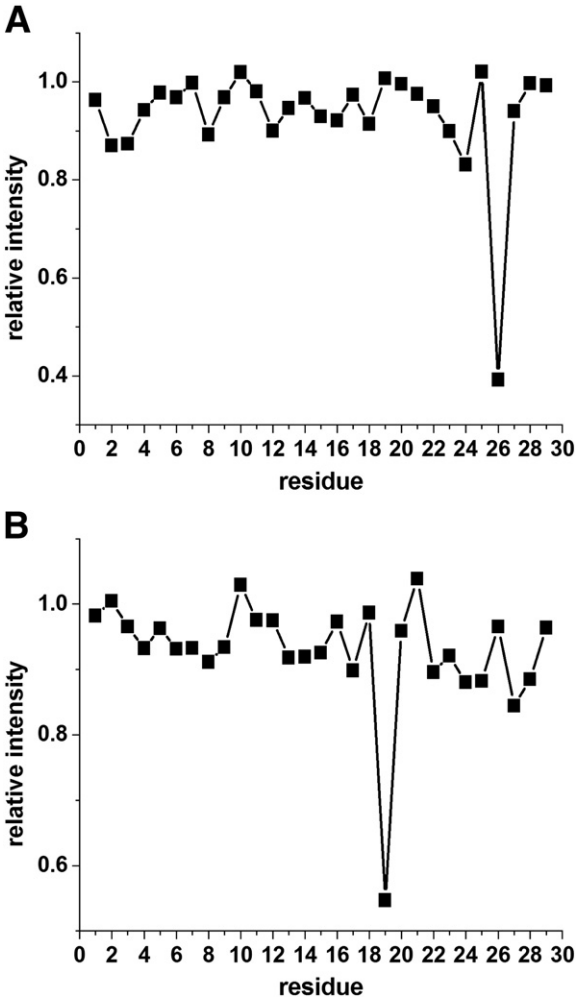

Fig. 8. Intensity of the most quenched cross-peak of each residue in the NOESY spectrum of D19A (A) and D26A (B) in SDS-d_{25} micelles at pH 5.5 in the presence of Co^{2+} relative to that in the absence of the metal ion.

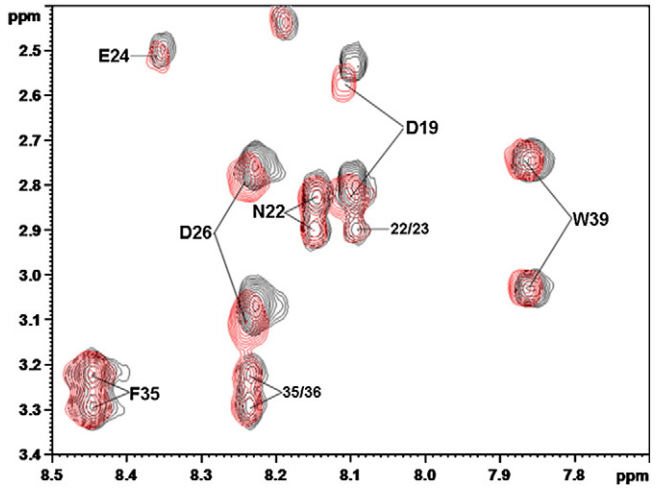

Fig. 10. Hβ-HN region of the NOESY spectrum of Nt-TMD1-loop1/2 in SDS-d_{25} micelles at pH 5.5 in the absence (black) and the presence (red) of Co^{2+}.

coordination to Co^{2+} by the residues Asp19, Glu24 and Asp26. This implies that the flexibility of the central part of TMD1 (especially DPGN motif) and the negatively charged residues in the motif and TMD1b may be important for the metal ion binding, and TMD1 can bind to divalent metal ions by the negatively charged residues whether TMD1b forms helix structure or not.

In the yeast homolog of DMT1 (SMF1 and SMF2), the residue corresponding to the Asp at position 93 of DMT1 is Ala that cannot provide polar side chain to interact with metal ions. This implies that the residue Asp93 (Asp26 in this study) may be not essential for the metal ion binding. Our results show that the D26A mutation does not affect the binding of Asp19 to Co^{2+} ion for the peptide TMD1 in SDS micelles, that is, the Asp19 can bind metal ions individually without the coordination of Asp26 side chain in the membrane-induced structure. Therefore, the residue Asp in DPGN motif may be more important for the uptake of Slc11 proteins to divalent metal ions in membrane. Although we cannot determine how other transmembrane segments are involved in the uptake of DMT1 to divalent metal ions, the significance of TMD1 in capturing divalent metal cations has been implicated in this study. The part of TMD1 near the surface of membrane may initially recognize divalent metal cations specifically, and then transfer them through channel by proton/metal ion coupling mechanism.

5. Conclusion

An α-helix-extended segment–α-helix structure of TMD1 in DMT1 was first confirmed experimentally in membrane-mimetic environments. The N-terminal part of TMD1 (including helix I) is deeply embedded in membrane, while the C-terminal part (including the motif DPGN and helix II) is close to the surface of membrane. TMD1 can bind metal ions, such as Co^{2+} and Mn^{2+}, by the side chains of the negatively charged residues in the C-terminal region. The flexibility of the central part of TMD1 (especially DPGN motif) and the negatively charged residue Asp86 wherein may be crucial for the metal ion binding. Either D19A or D26A (corresponding to D86A and D93A in DMT1) mutation does not affect the structure and metal ion binding of this membrane-spanning domain. The discontinuous helix structure of TMD1 may be intrinsic for Slc11 proteins and it can modulate the size of channel to accommodate and bind metal ions.

Acknowledgements

This work was financially supported by the NSFC (20973083 and 20934002).

Appendix A. Supplementary data

Supplementary data to this article can be found online at doi:10.1016/j.bbamem.2010.11.005.

References

[1] D.R. Richardson, P. Ponka, The molecular mechanisms of the metabolism and transport of iron in normal and neoplastic cells, Biochim. Biophys. Acta 1331 (1997) 1–40.
[2] Z.M. Qian, Q. Wang, P.L. Tang, Iron crossed the endosomal membrane by a carrier-mediated process, Prog. Biophys. Mol. Biol. 67 (1997) 1–15.
[3] E.C. Hirsch, Biochemistry of Parkinson's disease with special reference to the dopaminergic systems, Mol. Neurobiol. 9 (1994) 135–142.
[4] N.C. Andrews, Disorders of iron metabolism, New Engl. J. Med. 341 (1999) 1986–1995.
[5] S. Gruenheid, M. Cellier, S. Vidal, P. Gros, Identification and characterization of a second mouse Nramp gene, Genomics 25 (1995) 514–525.
[6] S. Vidal, D. Malo, K. Vogan, E. Skamene, P. Gros, Natural resistance to infection with intracellular parasites: isolation of a candidate for Bcg, Cell 73 (1993) 469–485.
[7] S. Vidal, P. Gros, E. Skamene, Natural resistance to infection with intracellular parasites: molecular genetics identifies Nramp1 as the Bcg/Ity/Lsh locus, J. Leuk. Biol. 58 (1995) 382–390.
[8] F. Canonne-Hergaux, S. Gruenheid, P. Ponka, P. Gros, Cellular and subcellular localization of the Nramp2 iron transporter in the intestinal brush border and regulation by dietary iron, Blood 93 (1999) 4406–4417.
[9] M.D. Fleming, C.C. Trenor III, M.A. Su, D. Foernzler, D.R. Beier, W.F. Dietrich, N.C. Andrews, Microcytic anaemia mice have a mutation in Nramp2, a candidate iron transporter gene, Nat. Genet. l6 (1997) 383–386.
[10] H. Gunshin, B. Mackenzie, U.V. Berger, Y. Gunshin, M.F. Romero, W.F. Boron, S. Nussberger, J.L. Gollan, M.A. Hediger, Cloning and characterization of a mammalian proton-coupled metal-ion transporter, Nature 388 (1997) 482–488.
[11] S.M. Vidal, E. Pinner, P. Lepage, S. Gauthier, P. Gros, Natural resistance to intracellular infections: Nramp1 encodes a membrane phosphoglycoprotein absent in macrophages from susceptible ($Nramp1^{D169}$) mouse strains, J. Immunol. 157 (1996) 3559–3568.
[12] M. Czachorowski, S. Lam-Yuk-Tseung, M. Cellier, P. Gros, Transmembrane topology of the mammalian Slc11a2 iron transporter, Biochemistry 48 (2009) 8422–8434.
[13] M. Cellier, G. Prive, A. Belouchi, T. Kwan, V. Rodrigues, W. Chia, P. Gros, Nramp defines a family of membrane proteins, Proc. Natl. Acad. Sci. U. S. A. 92 (1995) 10089–10093.
[14] H.A.H. Haemig, R.J. Brooker, Importance of conserved acidic residues in MntH, the Nramp homolog of Escherichia coli, J. Membr. Biol. 201 (2004) 97–107.
[15] S. Lam-Yuk-Tseung, G. Govoni, J. Forbes, P. Gros, Iron transport by Nramp2/DMT1: pH regulation of transport by 2 histidines in transmembrane domain 6, Blood 101 (2003) 3699–3707.
[16] A. Cohen, Y. Nevo, N. Nelson, The first external loop of the metal-ion transporter DCT1 is involved in metal-ion binding and specificity, Proc. Natl. Acad. Sci. U. S. A. 100 (2003) 10694–10699.
[17] Y. Song, D. Wang, H. Qi, S. Xiao, R. Xue, F. Li, Metal ion binding of the first external loop of DCT1 in aqueous solution, Metallomics 1 (2009) 392–394.
[18] P. Courville, E. Urbankova, C. Rensing, R. Chaloupka, M. Quick, M.F. Cellier, Solute carrier 11 cation symport requires distinct residues in transmembrane helices 1 and 6, J. Biol. Chem. 283 (2008) 9651–9658.
[19] A. Bax, D.G. Davis, MLEV-17-based two-dimensional homo-nuclear magnetization transfer spectroscopy, J. Magn. Reson. 65 (1985) 355–360.
[20] M. Piotto, V. Saudek, V. Sklenar, Gradient-tailored excitation for single-quantum NMR spectroscopy of aqueous solutions, J. Biol. NMR 2 (1992) 661–665.
[21] V. Sklenar, M. Piotto, R. Leppik, V. Saudek, Gradient-tailored water suppression for ^{1}H-^{15}N HSQC experiments optimized to retain full sensitivity, J. Magn. Reson. 102 (1993) 241–245.
[22] T.D. Goddard, D.G. Kneller, University of California, San Francisco, 2001.
[23] P. Güntert, C. Mumenthaler, K. Wüthrich, Torsion angle dynamics for NMR structure calculation with the new program DYANA, J. Mol. Biol. 273 (1997) 283–298.
[24] D.A. Pearlman, D.A. Case, J.W. Caldwell, W.S. Ross, T.E. Cheatham III, S. DeBolt, D. Ferguson, G. Seibel, P. Kollman, AMBER, a package of computer programs for applying molecular mechanics, normal mode analysis, molecular dynamics and free energy calculations to simulate the structural and energetic properties of molecules, Comput. Phys. Commun. 91 (1995) 1–41.
[25] W.D. Cornell, P. Cieplak, C.I. Bayly, I.R. Gould, K.M. Merz, D.M. Ferguson, D.C. Spellmeyer, T. Fox, J.W. Caldwell, P.A. Kollman, A second generation force field for the simulation of proteins, nucleic acids, and organic molecules, J. Am. Chem. Soc. 117 (1995) 5179–5197.
[26] R.A. Laskowski, J.A. Rullmann, M.W. MacArthur, R. Kaptein, J.M. Thornton, AQUA and PROCHECK-NMR: programs for checking the quality of protein structures solved by NMR, J. Biomol. NMR 8 (1996) 477–486.
[27] R. Koradi, M. Billeter, K. Wüthrich, MOLMOL: a program for display and analysis of macromolecular structures, J. Mol. Graph. 14 (1996) 51–55.
[28] M. Bisaglia, I. Tessari, L. Pinato, M. Bellanda, S. Giraudo, M. Fasano, E. Bergantino, L. Bubacco, S. Mammi, A topological model of the interaction between α-synuclein and sodium dodecyl sulfate micelles, Biochemistry 44 (2005) 329–339.
[29] M. Lindberg, J. Jarvet, U. Langel, A. Graslund, Secondary structure and position of the cell-penetrating peptide transportan in SDS micelles as determined by NMR, Biochemistry 40 (2001) 3141–3149.
[30] S. Xiao, J. Li, Y. Wang, C. Wang, R. Xue, S. Wang, F. Li, Identification of an "α-helix-extended segment–α-helix" conformation of the sixth transmembrane domain in DMT1, Biochim. Biophys. Acta 1798 (2010) 1556–1564.
[31] R. Chaloupka, P. Courville, F. Veyrier, B. Knudsen, T.A. Tompkins, M.F. Cellier, Identification of functional amino acids in the Nramp family by a combination of evolutionary analysis and biophysical studies of metal and proton co-transport in vivo, Biochemistry 44 (2005) 726–733.